LETTER

doi:10.1038/nature13498

The neurotrophic factor receptor RET drives haematopoietic stem cell survival and function

Diogo Fonseca-Pereira[1]*, Sílvia Arroz-Madeira[1]*, Mariana Rodrigues-Campos[1], Inês A. M. Barbosa[1], Rita G. Domingues[1], Teresa Bento[1], Afonso R. M. Almeida[1], Hélder Ribeiro[1], Alexandre J. Potocnik[2,3], Hideki Enomoto[4,5] & Henrique Veiga-Fernandes[1]

Haematopoiesis is a developmental cascade that generates all blood cell lineages in health and disease. This process relies on quiescent haematopoietic stem cells capable of differentiating, self renewing and expanding upon physiological demand[1,2]. However, the mechanisms that regulate haematopoietic stem cell homeostasis and function remain largely unknown. Here we show that the neurotrophic factor receptor RET (rearranged during transfection) drives haematopoietic stem cell survival, expansion and function. We find that haematopoietic stem cells express RET and that its neurotrophic factor partners are produced in the haematopoietic stem cell environment. Ablation of *Ret* leads to impaired survival and reduced numbers of haematopoietic stem cells with normal differentiation potential, but loss of cell-autonomous stress response and reconstitution potential. Strikingly, RET signals provide haematopoietic stem cells with critical *Bcl2* and *Bcl2l1* surviving cues, downstream of p38 mitogen-activated protein (MAP) kinase and cyclic-AMP-response element binding protein (CREB) activation. Accordingly, enforced expression of RET downstream targets, *Bcl2 or Bcl2l1*, is sufficient to restore the activity of *Ret* null progenitors *in vivo*. Activation of RET results in improved haematopoietic stem cell survival, expansion and *in vivo* transplantation efficiency. Remarkably, human cord-blood progenitor expansion and transplantation is also improved by neurotrophic factors, opening the way for exploration of RET agonists in human haematopoietic stem cell transplantation. Our work shows that neurotrophic factors are novel components of the haematopoietic stem cell microenvironment, revealing that haematopoietic stem cells and neurons are regulated by similar signals.

Haematopoietic stem cells (HSCs) are mostly quiescent in adulthood but can become proliferative upon physiological demand[1,2]. Autonomic nerves have been shown to be in close proximity to HSCs, raising the possibility that both cell types might be regulated through similar mechanisms[3–5]. Neurotrophic factors are key to neuron function and include the glial cell-line derived neurotrophic factor (GDNF) family of ligands (GFLs), which signal through the RET tyrosine kinase receptor in neurons, kidney and lymphoid cell subsets[6–8].

Initially we determined the expression of the canonical GFL receptor RET in fetal liver $Lin^-Sca1^+cKit^+$ (LSK) cells. When compared with myeloid progenitors ($Lin^-Sca1^-cKit^+$), LSKs expressed high levels of *Ret* and its co-receptors *Gfra1*, *Gfra2* and *Gfra3* (Extended Data Fig. 1a). *Ret* expression was higher in $Lin^-Sca1^+cKit^+CD150^+CD48^-$ haematopoietic stem cells (HSCs), while multipotent progenitors ($Lin^-Sca1^+cKit^+CD150^-CD48^+$) expressed this gene poorly (Fig. 1a)[6,8–10]. *Ret* expression by fetal HSCs was comparable to lymphoid tissue initiator cells (LTin), which are functionally dependent on RET (Fig. 1a, b)[6,11], while bone marrow HSCs expressed low levels of *Ret* (Extended Data Fig. 1b, c). Interestingly, cells known to support HSCs expressed the RET ligands GDNF, neurturin (NRTN) and artemin (ARTN) (Fig. 1c and Extended Data Fig. 1d, e)[12,13]. In agreement, the fetal liver and bone marrow HSC environment revealed the presence of GFLs in the vicinity of candidate HSCs, suggesting a role of RET in these cells (Fig. 1d, e and Extended Data Fig. 1f, g)[2].

To test this hypothesis we analysed *Ret* null mice[14]. Embryonic day (E)14.5 *Ret*-deficient LSKs and fetal liver cellularity were reduced in $Ret^{-/-}$ embryos (Fig. 1f and Extended Data Fig. 2a). However, the differentiation potential of $Ret^{-/-}$ LSKs was intact as revealed by normal colony-forming units (CFU) and *ex vivo* differentiation (Fig. 1g and Extended Data Fig. 2b.). Interestingly, *Ret* null LSKs were highly susceptible to apoptosis (Fig. 1h and Extended Data Fig. 2c) and *Ret* deficiency resulted in decreased HSC numbers with normal cell cycle profile (Fig. 1i, j and Extended Data Fig. 2d, e). These findings led us to investigate long-term HSC transplantation. Despite similar homing capacity (Extended Data Fig. 2f), *Ret*-deficient progenitors failed to rescue lethally irradiated mice (Fig. 1k).

To evaluate the fate of *Ret* null progenitors, we performed competitive transplantation assays. Fetal $Ret^{-/-}$ progenitors and wild type (WT) littermate controls were co-transplanted with equal numbers of third-party WT progenitors that ensured host survival (Fig. 2a). Analysis of recipient mice revealed that *Ret* null progenitors lost their transplantation fitness across all blood cell lineages (Fig. 2b and Extended Data Fig. 2g). Accordingly, bone marrow analysis 4 months after transplantation showed minute frequencies of *Ret*-deficient LSKs (Fig. 2c). Sequentially we performed highly sensitive secondary competitive transplantation assays with the same number of WT and $Ret^{-/-}$ bone marrow cells (Fig. 2a). We found minute frequencies of $Ret^{-/-}$ cells in the blood (Fig. 2d and Extended Data Fig. 2h), a defect already established in bone marrow LSKs (Fig. 2e). This major impact in long-term transplantation was in contrast to the modest reduction in the potential of short-term CFU-spleen (CFU-s) of $Ret^{-/-}$ progenitors (Extended Data Fig. 2i). Kidney and enteric nervous system development rely on activation of RET by GDNF and its co-receptor GDNF family receptor alpha 1 (GFRα1) (ref. 7). Analysis of E14.5 $Gfra1^{-/-}$, which similarly to $Ret^{-/-}$ animals die perinatally due to kidney aplasia, revealed normal progenitors and transplantation potential, suggesting that the $Ret^{-/-}$ HSC phenotype is not secondary to kidney or nervous system deficits (Extended Data Fig. 3). To address HSC-autonomous effects further, we generated Ret^{fl} mice that were bred to *Vav1*-iCre mice (Extended Data Fig. 4a)[8,15]. Deletion of the Ret^{fl} allele was inefficient in E14.5 HSCs[16], and *Vav1-i*Cre.Ret^{Δ} mice had normal fetal haematopoiesis (Extended Data Fig. 4b, c). In contrast, effective *Ret* conditional ablation led to reduced adult HSCs (Fig. 2f). In agreement, *Vav1-i*Cre.Ret^{Δ} mice died promptly upon 5-fluorouracil treatment (Fig. 2g). Primary and secondary transplantations also revealed that *Vav1-i*Cre.Ret^{Δ} progenitors lost their multi-lineage transplantation fitness (Fig. 2h and Extended Data Fig. 4d, e). Altogether, these results indicate that RET is a cell-autonomous requirement to HSC maintenance

[1]Instituto de Medicina Molecular, Faculdade de Medicina de Lisboa, Avenida Professor Egas Moniz, Edifício Egas Moniz, 1649-028 Lisboa, Portugal. [2]Division of Molecular Immunology, MRC National Institute for Medical Research, The Ridgeway, Mill Hill, London NW7 1AA, UK. [3]Institute of Immunology and Infection Research, University of Edinburgh, West Mains Road, Edinburgh EH9 3JT, UK. [4]Laboratory for Neuronal Differentiation and Regeneration, RIKEN Center for Developmental Biology, Kobe 650-0047, Japan. [5]Graduate School of Medicine, Kobe University7-5-1 Kusunoki-cho, Chuo-ku, Kobe City, Hyogo 650-0017, Japan.
*These authors contributed equally to this work.

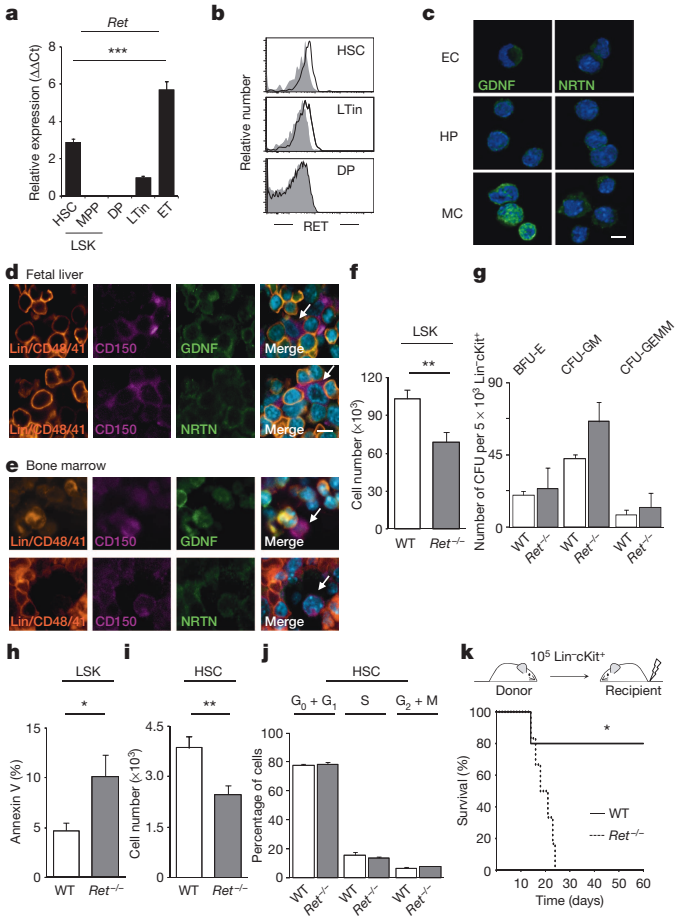

Figure 1 | *Ret* deficiency leads to reduced HSCs with impaired transplantation potential. **a**, E14.5 fetal liver HSCs and multipotent progenitor cells, double-positive thymocytes (DP), lymphoid tissue initiator cells (LTin) and adult enteric tissue (ET) were analysed by quantitative PCR with reverse transcription (RT–qPCR). ***P value for one-way analysis of variance (ANOVA) lower than 0.001. **b**, Flow cytometry of E14.5 fetal liver HSCs, LTin cells and double-positive thymocytes. Grey, isotype control. **c**, E14.5 fetal liver TER119$^-$CD45$^-$CD31$^+$ endothelial cells (EC), TER119$^-$CD45$^-$CD31$^-$cKit$^+$ ICAM-1$^-$ hepatocyte progenitors (HP) and TER119$^-$CD45$^-$CD31$^-$cKit$^-$ ICAM-1$^+$ mesenchymal cells (MC) were FACS-sorted and analysed by confocal microscopy. **d**, **e**, Confocal microscopy analysis. Arrows, Lin$^-$CD150$^+$CD48$^-$CD41$^-$ candidate HSCs. Scale bar, 5 µm. **f**, Fetal liver E14.5 LSKs. WT $n = 20$; $Ret^{-/-}$ $n = 18$. **g**, CFU per 5×10^3 Lin$^-$cKit$^+$ cells on day 8. BFU-E, burst-forming unit-erythrocyte; CFU-GM, colony-forming unit-granulocyte/macrophage; CFU-GEMM, colony-forming unit-granulocyte/erythrocyte/macrophage/megakaryocyte. WT $n = 3$; $Ret^{-/-}$ $n = 3$. **h**, Annexin V$^+$ cells in cultured LSKs. WT $n = 7$; $Ret^{-/-}$ $n = 4$. **i**, E14.5 HSCs. WT $n = 20$; $Ret^{-/-}$ $n = 18$. **j**, HSC cell cycle. WT $n = 7$; $Ret^{-/-}$ $n = 6$. **k**, Survival upon transplantation. *P value for log rank test lower than 0.05. WT $n = 5$; $Ret^{-/-}$ $n = 6$. Error bars, s.e.m. * and **, P values for Student's t-test lower than 0.05 and 0.01 respectively.

and haematopoietic stress responses, a finding also supported by *Ret* upregulation after irradiation-induced genotoxic stress (Extended Data Fig. 5a).

Previous reports have identified a gene signature associated with long-term HSC activity[17–19]. While most of those genes were not significantly modified, *Bcl2* and *Bcl2l1* were heavily reduced in *Ret* null LSKs and HSCs (Fig. 3a, b and Extended Data Fig. 5b, c). The marked reduction of BCL2 and BCLxL, together with the susceptibility of $Ret^{-/-}$ progenitors to apoptosis, suggested that GFLs could provide survival signals to HSCs. In agreement, GFLs increased blood progenitor survival and preserved HSCs in culture conditions (Fig. 3c, d and Extended Data Fig. 5d).

RET activation in neurons leads to ERK1/2, PI3K/Akt and p38/MAP kinase activation[7], while phosphorylation of CREB induces *Bcl2* gene

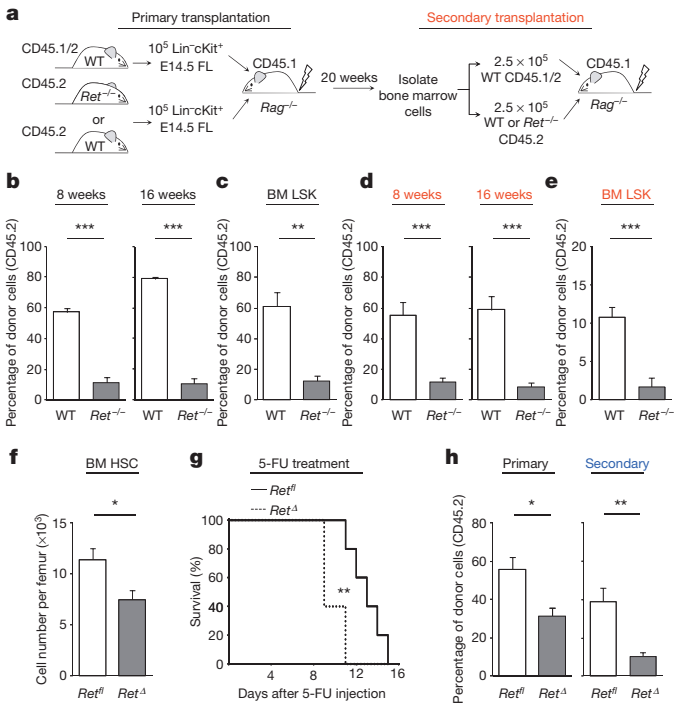

Figure 2 | RET cell-autonomous signals control haematopoietic stress responses. **a**, Primary and secondary (red) transplantation. FL, fetal liver. **b**, Donor CD45.2 blood cells in primary transplantations. WT $n = 5$; $Ret^{-/-}$ $n = 9$. Representative of two independent experiments. **c**, Donor bone marrow (BM) CD45.2 LSK cells. WT $n = 3$; $Ret^{-/-}$ $n = 4$. **d**, Donor CD45.2 cells after serial transplantation. WT $n = 5$; $Ret^{-/-}$ $n = 4$. Representative of two independent experiments. **e**, Donor bone marrow CD45.2 LSK after serial transplantation. WT $n = 5$; $Ret^{-/-}$ $n = 4$. **f**, Bone marrow HSCs in Ret^{Δ} and Ret^{fl} littermate controls. Ret^{fl} $n = 10$; Ret^{Δ} $n = 7$. **g**, Survival after treatment with 5-fluorouracil (5-FU). Ret^{fl} $n = 5$; Ret^{Δ} $n = 5$. **P value for log rank test lower than 0.01. **h**, Donor blood cells 16 weeks after primary and secondary (blue) transplantation. Primary: Ret^{fl} $n = 5$; Ret^{Δ} $n = 4$; secondary: Ret^{fl} $n = 7$; Ret^{Δ} $n = 9$. Similar results were obtained in two independent experiments. Error bars, s.e.m. *, ** and ***, P values for Student's t-test lower than 0.05, 0.01 and 0.001 respectively.

family expression[20,21]. Analysis of p38/MAP kinase and CREB in $Ret^{-/-}$ LSKs revealed that these molecules were hypo-phosphorylated, while ERK1/2 and PI3K/Akt activation was unperturbed (Fig. 3e and Extended Data Fig. 5e). Accordingly, RET activation by GFLs led to rapid p38/MAP kinase and CREB phosphorylation and increased *Bcl2*/*Bcl2l1* expression by LSKs, while ERK1/2, PI3K/Akt phosphorylation was stable (Fig. 3f, g and Extended Data Fig. 5f). Importantly, inhibition of p38/MAP kinase upon GFL activation led to impaired CREB phosphorylation and *Bcl2*/*Bcl2l1* expression while inhibition of ERK1/2 and PI3K/Akt had no impact on these molecules (Fig. 3h, i and Extended Data Fig. 5g). Finally, inhibition of CREB upon GFL activation resulted in decreased *Bcl2*/*Bcl2l1* levels (Fig. 3j). Altogether, these data demonstrate that RET-deficient LSKs express reduced *Bcl2* and *Bcl2l1*, downstream of impaired p38/MAP kinase and CREB activation; this is a signalling pathway that was also operational in purified HSCs (Fig. 3k).

These findings suggested that reduced *Bcl2* and *Bcl2l1* caused the unfitness of *Ret*-deficient HSC. Retroviral transductions showed that *Bcl2* and *Bcl2l1* expression levels were quickly restored in $Ret^{-/-}$ LSKs transduced with WT *Ret*, while other signature genes were unperturbed (Fig. 4a). To test whether $Ret^{-/-}$ progenitor fitness could be restored by enforced *Ret* expression, we performed competitive transplantations with $Ret^{-/-}$ progenitors transduced with pMig.*Ret9*.IRES–GFP (IRES, internal ribosomal entry site; GFP, green fluorescent protein) retrovirus together with competitor CD45.1 bone marrow (Extended Data Fig. 6a). Restoration of RET expression fully rescued $Ret^{-/-}$ progenitor transplantation (Fig. 4b, c), and enforced expression of RET downstream

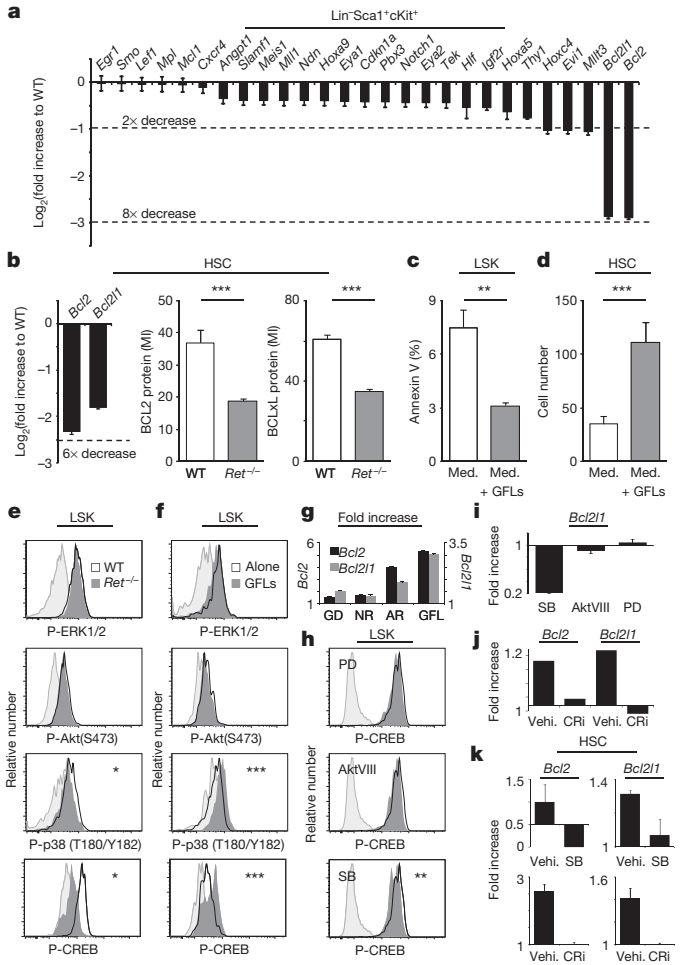

Figure 3 | RET induces *Bcl2*/*Bcl2l1* downstream of p38/MAP and CREB activation. **a**, Fetal liver E14.5 $Ret^{-/-}$ and WT LSKs ($n = 3$). **b**, Left, fetal liver E14.5 $Ret^{-/-}$ and WT HSCs ($n = 3$). Right, mean intensity (MI) for BCL2 and BCLxL protein in fetal liver E14.5 $Ret^{-/-}$ and WT HSCs. BCL2: WT $n = 40$, $Ret^{-/-}$ $n = 29$; BCLxL: WT $n = 40$, $Ret^{-/-}$ $n = 40$. **c**, Annexin V$^+$ LSK cells cultured in medium (Med.) with or without GFLs ($n = 9$). **d**, HSC numbers after GFL treatment ($n = 12$). **e**, E14.5 $Ret^{-/-}$ and WT littermate control LSKs. P-ERK and P-Akt: WT $n = 15$, $Ret^{-/-}$ $n = 16$; P-p38: WT $n = 3$, $Ret^{-/-}$ $n = 3$; P-CREB: WT $n = 16$, $Ret^{-/-}$ $n = 19$. **f**, LSK activation by GFLs. P-ERK and P-Akt: alone $n = 12$, GFLs $n = 12$; P-p38: alone $n = 12$, GFLs $n = 12$; P-CREB: alone $n = 6$, GFLs $n = 6$. **g**, LSKs upon treatment with GDNF (GD), NRTN (NR), ARTN (AR) and three GFLs (GFL). Relative to PBS-treated LSKs (vehicle). **h**, LSKs cultured with GFLs (black line) or GFLs and the inhibitors SB 202190 (SB), PD98,059 (PD) or Akt1/2, Akt Inhibitor VIII (AktVIII) (solid grey). PD, AktVIII and SB: GFLs $n = 6$, GFLs+inh $n = 6$. **i**, LSK cells upon GFL treatment. Relative to GFL-treated LSKs. **j**, Treatment with GFLs + DMSO (vehicle (Vehi.)) or GFLs + CBP-CREB interaction inhibitor (CRi), relative to DMSO-treated LSKs (vehicle). **k**, HSCs after treatment with GFL+DMSO (vehicle), GFL+SB 202190 (SB) or GFL+CBP-CREB interaction inhibitor (CRi), relative to DMSO-treated HSCs (vehicle). Error bars, s.e.m. Light grey, isotype control. **and ***, *P* values for Student's *t*-test lower than 0.01 and 0.001 respectively.

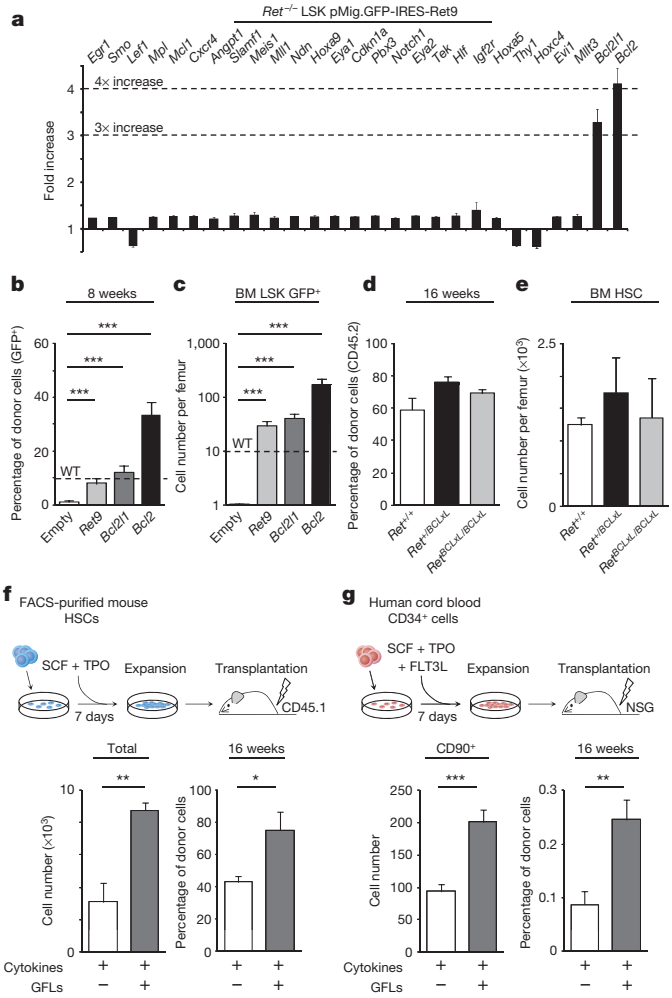

Figure 4 | RET activation promotes HSC expansion and transplantation efficiency. **a**, Fold increase between $Ret^{-/-}$ pMig–GFP–IRES-*Ret9* and empty vector ($n = 3$). **b**, CD45.2$^+$GFP$^+$ blood cells 8 weeks after transplantation with $Ret^{-/-}$ progenitors transduced with pMig–GFP–IRES-Empty (Empty) virus, or expressing *Ret9*, *Bcl2l1* or *Bcl2*. Empty $n = 13$; *Ret9* $n = 5$; *Bcl2l1* $n = 8$; *Bcl2* ($n = 7$). **c**, Bone marrow LSKs. $Ret^{-/-}$ Empty $n = 13$; *Ret9* $n = 4$; *Bcl2l1* $n = 6$; *Bcl2* ($n = 5$). **d**, Donor CD45.2 blood cells 16 weeks after competitive transplantation. $Ret^{+/+}$ ($n = 8$); $Ret^{+/BCLxL}$ $n = 8$; $Ret^{BCLxL/BCLxL}$ $n = 8$. Similar results were obtained in two independent experiments. **e**, Bone marrow CD45.2 HSCs 16 weeks after transplantation. $Ret^{+/+}$ $n = 3$; $Ret^{+/BCLxL}$ $n = 3$; $Ret^{BCLxL/BCLxL}$ $n = 3$. Similar results were obtained in two independent experiments. **f**, Purified HSCs were expanded for 7 days with or without GFLs and were transplanted with competitor CD45.1 bone marrow cells. Bottom left: nucleated cells at culture day 7 ($n = 11$). Bottom right: culture-derived blood cells (CD45.2) at 16 weeks after transplantation ($n = 5$). Similar results were obtained in two independent experiments. **g**, Top: scheme expansion and transplantation of human CD34$^+$ cells. Bottom left: CD34$^+$CD38$^-$CD90$^+$ cells at culture day 7 ($n = 20$). Bottom right: culture-derived hCD45$^+$ blood cells at 16 weeks after transplantation ($n = 5$). Similar results were obtained in two independent experiments. Error bars, s.e.m. *, **and ***, *P* values for Student's *t*-test lower than 0.05, 0.01 and 0.001 respectively.

targets, *Bcl2* or *Bcl2l1*, was sufficient to recover the engraftment of *Ret* null LSKs but had no effect on their WT counterparts (Fig. 4b, c and Extended Data Fig. 6b). Since retroviral expression became unstable *in vivo*, we generated a knock-in mouse expressing *BCL2L1* under the control of *Ret* (Ret^{BCLxL}) (Extended Data Fig. 7a). Ret^{BCLxL} heterozygous mice had increased *BCL2L1* expression but displayed normal haematopoiesis and HSCs (Extended Data Fig. 7b, c). *Ret*-deficient mice expressing ectopic *BCL2L1* ($Ret^{BCLxL/BCLxL}$) had normal fetal progenitors (Extended Data Fig. 7b, d) and transplantation of these progenitors was similar to WT levels at week 16 (Fig. 4d, e and Extended Data Fig. 7e). These data indicate that *Bcl2l1* has no significant impact in WT progenitors but is sufficient to restore the function of *Ret* null progenitors.

Evidence that RET signals promote HSC expansion was provided by *in vitro* cultures of fluorescence-activated cell sorting (FACS)-purified HSCs with stem cell factor, thrombopoietin and GFLs. Addition of GFLs to purified HSCs improved their expansion (Fig. 4f); and transplantation of expanded HSCs revealed that GFL-treated HSCs had increased fitness (Fig. 4f). Remarkably, addition of GFLs to human cord blood CD34$^+$ progenitors significantly increased *BCL2* and *BCL2L1* expression; improved expansion of primitive progenitors and resulted in increased

repopulation activity of human progenitors into NOD.Cg-*Prkdc*^{scid} *Il2rg*^{tm1Wjl}/SzJ (NSG) mice (Fig. 4g and Extended Data Fig. 8).

Our results reveal that RET signalling is a crucial cell-autonomous pathway controlling fetal and adult HSC survival via BCL2 family members. Previous studies have identified molecules that co-regulate HSC maintenance and differentiation[1,2,17–19]. We now show that RET activation by GFLs specifically regulates HSC survival, preserving HSC stemness and discriminating between HSC maintenance and progenitor differentiation. Despite *Bcl2* expression by HSCs, no appreciable LSK transplantation deficiencies were reported in *Bcl2*-deficient mice, although reduced haematopoietic precursors were reported in *Bcl2l1*$^{-/-}$ mice[22,23]. Thus, *Bcl2* and *Bcl2l1* may have redundant roles in HSCs, an idea supported by our data demonstrating that *Bcl2l1* or *Bcl2* are independently sufficient to rescue *Ret*$^{-/-}$ HSCs (Fig. 4b–e). Contrary to nervous cells, we suggest that HSCs use GFLs in a redundant manner[11] since analysis of RET co-receptor single knockouts revealed normal LSKs (Extended Data Fig. 3 and Extended Data Fig. 9)[24–26].

Our study indicates that absence of neurotrophic factor cues leads to impaired HSC survival and transplantation. Accordingly, activation of RET results in improved HSC survival, expansion and *in vivo* transplantation efficiency. Thus, we propose that RET controls HSC response to physiological demands (Extended Data Fig. 10). Altogether, these findings open new horizons for pre-clinical testing of GFLs in human haematopoietic progenitor expansion and transplantation.

Previous work revealed that nervous cells modulate HSC function[3–5,27–29]; we now show that HSCs are direct targets for neurotrophic factors, indicating that HSCs and neurons are regulated by similar signals. Thus, our work puts forward a possible regulation of neuronal activity by primitive blood progenitors through neurotrophic factor consumption in the HSC environment.

METHODS SUMMARY

Mice were bred and maintained at the Instituto de Medicina Molecular animal facility. Lin$^-$cKit$^+$ cells were MACS (Miltenyi Biotec) sorted and injected alone or in direct competition with a third-party WT competitor CD45.1/CD45.2 into lethally irradiated CD45.1 mice. Secondary reconstitution experiments were performed on FACS-sorted bone marrow cells from primary recipients and injected intravenously with third-party cells. FACS-sorted murine HSCs were cultured for 7 days in StemSpan SFEM (STEMCELL Technologies). Human cord blood CD34$^+$ cells were cultured similarly to murine HSCs, with added rmFLT3.

Online Content Methods, along with any additional Extended Data display items and Source Data, are available in the online version of the paper; references unique to these sections appear only in the online paper.

Received 27 June 2012; accepted 21 May 2014.
Published online 27 July 2014.

1. Trumpp, A., Essers, M. & Wilson, A. Awakening dormant haematopoietic stem cells. *Nature Rev. Immunol.* **10,** 201–209 (2010).
2. Morrison, S. J. & Scadden, D. T. The bone marrow niche for haematopoietic stem cells. *Nature* **505,** 327–334 (2014).
3. Yamazaki, S. *et al.* Nonmyelinating Schwann cells maintain hematopoietic stem cell hibernation in the bone marrow niche. *Cell* **147,** 1146–1158 (2011).
4. Mendez-Ferrer, S., Lucas, D., Battista, M. & Frenette, P. S. Haematopoietic stem cell release is regulated by circadian oscillations. *Nature* **452,** 442–447 (2008).
5. Lucas, D. *et al.* Chemotherapy-induced bone marrow nerve injury impairs hematopoietic regeneration. *Nature Med.* **19,** 695–703 (2013).
6. Veiga-Fernandes, H. *et al.* Tyrosine kinase receptor RET is a key regulator of Peyer's Patch organogenesis. *Nature* **446,** 547–551 (2007).
7. Mulligan, L. M. RET revisited: expanding the oncogenic portfolio. *Nature Rev. Cancer* **14,** 173–186 (2014).
8. Almeida, A. R. *et al.* RET/GFRα signals are dispensable for thymic T cell development *in vivo*. *PLoS ONE* **7,** e52949 (2012).
9. Kiel, M. J., Yilmaz, O. H., Iwashita, T., Terhorst, C. & Morrison, S. J. SLAM family receptors distinguish hematopoietic stem and progenitor cells and reveal endothelial niches for stem cells. *Cell* **121,** 1109–1121 (2005).
10. Kim, I., He, S., Yilmaz, O. H., Kiel, M. J. & Morrison, S. J. Enhanced purification of fetal liver hematopoietic stem cells using SLAM family receptors. *Blood* **108,** 737–744 (2006).
11. Patel, A. *et al.* Differential RET signaling pathways drive development of the enteric lymphoid and nervous systems. *Sci. Signal.* **5,** ra55 (2012).
12. Winkler, I. G. *et al.* Positioning of bone marrow hematopoietic and stromal cells relative to blood flow *in vivo*: serially reconstituting hematopoietic stem cells reside in distinct nonperfused niches. *Blood* **116,** 375–385 (2010).
13. Ding, L. & Morrison, S. J. Haematopoietic stem cells and early lymphoid progenitors occupy distinct bone marrow niches. *Nature* **495,** 231–235 (2013).
14. Schuchardt, A., D'Agati, V., Larsson-Blomberg, L., Costantini, F. & Pachnis, V. Defects in the kidney and enteric nervous system of mice lacking the tyrosine kinase receptor Ret. *Nature* **367,** 380–383 (1994).
15. de Boer, J. *et al.* Transgenic mice with hematopoietic and lymphoid specific expression of Cre. *Eur. J. Immunol.* **33,** 314–325 (2003).
16. McMahon, K. A. *et al.* MII has a critical role in fetal and adult hematopoietic stem cell self-renewal. *Cell Stem Cell* **1,** 338–345 (2007).
17. Mansson, R. *et al.* Molecular evidence for hierarchical transcriptional lineage priming in fetal and adult stem cells and multipotent progenitors. *Immunity* **26,** 407–419 (2007).
18. Terskikh, A. V., Miyamoto, T., Chang, C., Diatchenko, L. & Weissman, I. L. Gene expression analysis of purified hematopoietic stem cells and committed progenitors. *Blood* **102,** 94–101 (2003).
19. Thompson, B. J. *et al.* Control of hematopoietic stem cell quiescence by the E3 ubiquitin ligase Fbw7. *J. Exp. Med.* **205,** 1395–1408 (2008).
20. Perianayagam, M. C., Madias, N. E., Pereira, B. J. & Jaber, B. L. CREB transcription factor modulates Bcl2 transcription in response to C5a in HL-60-derived neutrophils. *Eur. J. Clin. Invest.* **36,** 353–361 (2006).
21. Shukla, A. *et al.* Activated cAMP response element binding protein is overexpressed in human mesotheliomas and inhibits apoptosis. *Am. J. Pathol.* **175,** 2197–2206 (2009).
22. Nakayama, K., Negishi, I., Kuida, K., Sawa, H. & Loh, D. Y. Targeted disruption of Bcl-2αβ in mice: occurrence of gray hair, polycystic kidney disease, and lymphocytopenia. *Proc. Natl Acad. Sci. USA* **91,** 3700–3704 (1994).
23. Motoyama, N. *et al.* Massive cell death of immature hematopoietic cells and neurons in Bcl-x-deficient mice. *Science* **267,** 1506–1510 (1995).
24. Cacalano, G. *et al.* GFRα1 is an essential receptor component for GDNF in the developing nervous system and kidney. *Neuron* **21,** 53–62 (1998).
25. Nishino, J. *et al.* GFR α3, a component of the artemin receptor, is required for migration and survival of the superior cervical ganglion. *Neuron* **23,** 725–736 (1999).
26. Rossi, J. *et al.* Retarded growth and deficits in the enteric and parasympathetic nervous system in mice lacking GFR α2, a functional neurturin receptor. *Neuron* **22,** 243–252 (1999).
27. Katayama, Y. *et al.* Signals from the sympathetic nervous system regulate hematopoietic stem cell egress from bone marrow. *Cell* **124,** 407–421 (2006).
28. Mendez-Ferrer, S. *et al.* Mesenchymal and haematopoietic stem cells form a unique bone marrow niche. *Nature* **466,** 829–834 (2010).
29. Spiegel, A. *et al.* Catecholaminergic neurotransmitters regulate migration and repopulation of immature human CD34+ cells through Wnt signaling. *Nature Immunol.* **8,** 1123–1131 (2007).

Acknowledgements We thank I. Monteiro Grillo and the radiotherapy service at Hospital de Santa Maria; H. Ferreira and the service of obstetrics, gynaecology and reproductive medicine at the Hospital of Santa Maria; the Instituto de Medicina Molecular animal facility, flow cytometry unit, bioimaging unit and histology unit for technical assistance. We also thank all members of H.V.-F. laboratory for discussion. D.F.-P., S.A.-M., R.G.D. and A.R.M.A. were supported by scholarships from Fundação para a Ciência e Tecnologia, Portugal. H.V.-F. was supported by Fundação para a Ciência e Tecnologia (PTDC/SAU-MII/104931/2008), Portugal, the European Molecular Biology Organisation (Project 1648), European Research Council (Project 207057) and National Blood Foundation, USA.

Author Contributions D.F.-P., S.A.-M., M.R.-C., I.B., R.G.D., T.B., A.R.M.A. and H.R. did experiments and data analysis; H.E. generated *Ret*^{BCLxL} mice; D.F.-P., S.A.-M., A.P. and H.V.-F. designed *in vivo* and *ex vivo* experiments; D.F.-P. and H.V.-F. wrote the manuscript and H.V.-F. directed the study.

Author Information Reprints and permissions information is available at www.nature.com/reprints. The authors declare no competing financial interests. Readers are welcome to comment on the online version of the paper. Correspondence and requests for materials should be addressed to H.V.-F. (jhfernandes@medicina.ulisboa.pt).

METHODS

Mice. C57BL/6J (CD45.2 and CD45.1), *Rag1*$^{-/-}$ (CD45.2 and CD45.1)[30], *Vav1*iCre[15], *Gfra1*$^{-/-}$ (ref. 24), *Gfra2*$^{-/-}$ (ref. 26), *Gfra3*$^{-/-}$ (ref. 25), *Ret*$^{-/-}$ (ref. 14) and *Ret*^{fl} (ref. 8) were maintained at the Instituto de Medicina Molecular. NSG mice were bought from The Jackson Laboratory. *Ret*$^{BCLxL-IRES-Puro}$ (*Ret*^{BCLxL}) knock-in mice were generated by inserting a gene cassette composed of human *BCL2L1* complementary DNA (cDNA) followed by ires-puromycin resistance gene into the endogenous *Ret* locus via gene targeting as describe previously[31]. We performed power analysis to determine sample size. No exclusion, blinding or randomization criteria were used in experiments involving genetically modified animals. Mice were systematically compared with sex-matched littermate controls. All mice strains were bred and maintained at the Instituto de Medicina Molecular animal facility. Animal procedures were in accordance with national and institutional guidelines.

Colony-forming unit assays and homing capacity. Five thousand E14.5 Lin$^-$cKit$^+$ cells were MACS purified (Miltenyi Biotec) from WT and *Ret*$^{-/-}$ and cultured in M3434 (Stem Cell Technologies), and scored at days 8–10 by flow cytometry and microscope analysis. Thirty thousand E14.5 Lin$^-$cKit$^+$ cells were MACS (Miltenyi Biotec) purified from WT or *Ret*$^{-/-}$, injected into lethally irradiated mice (9 Gy) and CFU-s scored at day 12 by microscope analysis. Homing assays used E14.5 Lin$^-$cKit$^+$ cells labelled with CMTMR (Invitrogen), injected into lethally irradiated mice. We performed flow cytometry analysis 20 h after injection.

Transplantation experiments. For reconstitution experiments with fetal liver, 1×10^5 E14.5 Lin$^-$cKit$^+$ cells were MACS sorted from WT, *Ret*$^{-/-}$, *Ret*$^{+/BCLxL}$ or *Ret*$^{BCLxL/BCLxL}$ and were injected alone or in direct competition with a third-party WT competitor CD45.1/CD45.2 (1:1 ratio) into lethally irradiated *Rag1*$^{-/-}$ CD45.1 mice. For secondary reconstitution experiments with bone marrow, 2.5×10^5 cells from each genotype were FACS-sorted from primary recipients and injected intravenously in competition with the WT CD45.1/CD45.2 third-party competitor cells into lethally irradiated *Rag1*$^{-/-}$ CD45.1 mice. *Vav1-i*Cre.*Ret*$^{\Delta}$ competitive transplants were analysed at 16 weeks after transplantation of 2.5×10^5 cells from each genotype together with CD45.1/CD45.2 competitor WT cells.

Rescue of *in vivo* transplantation. E14.5 Lin$^-$cKit$^+$Sca1$^+$ WT or *Ret*$^{-/-}$ cells were transduced overnight with pMig.IRES–GFP retroviral vector containing *Ret9*, *Bcl2* or *Bcl2l1*. GFP$^+$ cells were further FACS purified for immediate transcriptional analysis. Lin$^-$cKit$^+$GFP$^+$ cells were injected into lethally irradiated mice. Six weeks later transduced bone marrow Lin$^-$CD45.2$^+$GFP$^+$ cells were purified by flow cytometry and 10^5 cells were co-injected with a radio-protective dose of 10^5 CD45.1 bone marrow cells into lethally irradiated recipients.

5-Fluorouracil treatment. *Vav1-i*Cre.*Ret*$^{\Delta}$ and their littermate controls were injected weekly with 150 μg of 5-fluorouracil per gram of body weight.

Flow cytometry. Embryonic fetal livers were micro-dissected and homogenized in 70 μm cell strainers. Bone marrow cells were either collected by flushing or crushing bones. Bone marrow cells numbers were calculated per femur. Cell suspensions were stained with: anti-CD117 (cKit) (2B8), anti-Ly-6A/E (Sca-1) (D7), anti-CD16/32 (FcRγII/III) (93), anti-CD3 (eBio500A2), anti-CD150 (mShad150), anti-CD48 (HM48-1), anti-CD19 (eBio1D3), anti-CD11b (M1/70), anti-Ly-6G (Gr-1) (RB6-8C5), anti-Ly79 (TER119), anti-NK1.1 (PK136), anti-CD11c (N418), anti-CD45.1 (A20), anti-CD45.2 (104), anti-CD54 (ICAM-1) (YN1/1.7.4), anti-CD34 (RAM34), anti-CD51 (RMV-7) and anti-CD41 (eBioMWReg30) from eBioscience; anti-CD38 (90), anti-CD3 (145-2C11), anti-CD34 (HM34) and anti-CD31 (390) from BioLegend; anti-Ly6C (HK1.4) from Abcam, Annexin V from BD Pharmingen. Lineage cocktail include anti-CD3, anti-CD19, anti-Ly-6G, anti-Ly6C, anti-Ly79, anti-NK1.1, anti-CD11c for embryonic fetal livers plus anti-CD11b for adult bone marrow cells. HSCs were defined as Lin$^-$Sca1$^+$cKit$^+$CD150$^+$CD48$^-$ cells, LSKs as Lin$^-$Sca1$^+$cKit$^+$ cells and myeloid progenitors were defined as Lin$^-$Sca1$^-$cKit$^+$ cells. Human cord blood was enriched for CD34$^+$ cells using CD34 MicroBead Kit (Miltenyi Biotec) after Histopaque separation (Sigma) and stained with anti-human CD34 (AC136) (Miltenyi Biotec), anti-human CD38 (HIT2) (eBioscience), anti-human CD45 (HI30) (eBioscience) and anti-human CD90 (5E10) (eBioscience). Samples were sorted on a FACSAria I or FACSAria III and analysed on a FACSCanto or LSRFortessa (BD). We analysed flow cytometry data with FlowJo 8.8.7 software (Tree Star).

Immunofluorescence of sorted cells. Two thousand to forty thousand cells were seeded in poly-lysine coated coverslips (Sigma Aldrich P8920). Cells were fixed for 15 min in 2% PFA at 4 °C or 10 min with methanol at −20 °C (for BCLxL staining). Slides were then washed with PBS, permeabilized with 0.15% Triton X-100 for 10 min at 4 °C and stained in 3% FBS for 45 min at 4 °C with anti-RET (Neuromics GT15002), anti-GDNF (Abcam 18956), anti-Neurturin (R&D Systems AF477), anti-Artemin (R&D Systems 185234), anti-mouse BCL2 (3F11) (BD Pharmingen) or anti-BCLxL (H-62) (Santa Cruz biotechnology). Secondary antibody staining plus DAPI was done for 30 min at 4 °C using anti-rabbit (Invitrogen A21206), anti-mouse (Invitrogen A21127), anti-goat (Invitrogen A11078), anti-rat (Invitrogen A11006) or anti-Armenian hamster (Jackson ImmunoResearch 127-165-099). Slides were mounted in Mowiol (Calbiochem), images acquired on a Zeiss LSM 710 (×63 objective) and images analysed using ImageJ software.

Histology and immunofluorescence. Whole-mount bone marrow samples were prepared as previously described[32]. Briefly, sternal bones were collected and transected with a surgical blade into two or three fragments. Fragments were bisected sagittally for the bone marrow cavity to be exposed, fixed in 4% PFA and blocked and permeabilized in 1× PBS with 2% BSA, 10% FBS, 0.6% Triton X-100, followed by an Avidin/Biotin Blocking Kit (Vector laboratories).

Frozen section preparation. Femurs were placed in 4%PFA for 2 h at 4 °C and imbued overnight in 30% sucrose. Bones were then included in Cutting Temperature (OCT) compound (Sakura), snap frozen in *N*-methylbutane chilled in liquid nitrogen and kept at −80 °C. Sections (7 μm) obtained using a Cryostat LEICA CM 3050S with a tungsten carbide blade were placed in coated slides. E14.5 fetal liver or E15.5 enteric tissue were placed in 4% PFA overnight at 4 °C followed imbedding in 10% (2 h), 20% (2 h) and 30% sucrose (overnight). Fetal liver or enteric tissue were then included in OCT, frozen in dry ice and kept at −30 °C. Sections (10 μm) obtained using a Cryostat LEICA CM 3050S were placed on coated slides. Slides were air dried, rinsed with PBS and blocked for 30 min at room temperature with 1× PBS, 2% BSA, 10% FBS. Then sections were washed and blocked using an Avidin/Biotin Blocking Kit (Vector laboratories), and permeabilized with PBS 0.3% Triton X-100 for 10 min at room temperature (about 22 °C).

Immunofluorescence staining of whole-mount tissues and frozen sections. Slides or samples were incubated overnight (or for 1–2 days for the whole-mount samples), at 4 °C with biotin-labelled antibodies in PBS: CD3 (eBio500A2), anti-CD19 (eBio1D3), anti-Ly79 (TER119), anti-Ly-6G (Gr-1), anti-CD11c (N418), anti-CD41 (eBioMWReg30) and anti-CD48 (HM48-1); together with anti-CD150 (mShad150) Alexa Fluor 488 and with either one of the following primary antibodies: anti-GDNF (Abcam 18956), anti-Neurturin (R&D Systems AF477) or anti-Artemin (R&D Systems 185234). Samples were then washed in 1× PBS, 2% BSA, 10% FBS and stained with Streptavidin A546-conjugated (Invitrogen S11225) together with either A647 anti-rabbit (Invitrogen A21244), anti-goat (Invitrogen A21447), anti-rat (Invitrogen A21247) or A405 anti-rabbit (abcam ab175652) secondary antibodies plus DAPI for 45 min at room temperature (or 2½ h plus TOPRO3 (Invitrogen) for whole-mount samples). Samples were washed with 1× PBS, 2% BSA, 10% FBS and bone marrow, fetal liver and enteric tissue sections were mounted using Mowiol (Calbiochem 475904) while whole-mount samples were dehydrated in methanol and optically cleared using benzyl alcohol:benzyl benzoate (BABB) (Sigma)[6,33]. Sections or whole-mount images were aquired with a Zeiss LSM 710 (×40 or ×63 objective lens for whole-mount or frozen sections respectively) and images were processed using Zeiss LSM Image Browser (Carl Zeiss).

Intracellular staining. Intracellular staining used BrdU Flow Kit, anti-P-S6 (pS235/pS236) (N7-548) and anti-P-Akt (pT308) (JI-223.371) from BD Pharmingen, anti-PIP_3 (Z-P345) from Echelon Biosciences, and anti-P-CREB (pS133) (87G3), anti-P-p38 (pT180/Y182) (28B10), anti-P-Akt (pS473) (D9E) and anti-P-ERK1/2 (pT202/pY204) (D13.14.4E) from Cell Signaling Technology. Intracellular staining used anti-human RET (132507) from R&D Systems according to the manufacturer's instructions.

Signalling and cell death. One million E14.5 WT Lin$^-$cKit$^+$ cells were cultured in DMEM and starved for 2 h. To test CREB phosphorylation upon GFL stimulation Lin$^-$cKit$^+$ cells were stimulated for 1 h with 500 ng ml^{-1} each of GFL and co-receptor (rrGFR-α1, rmGFR-α2, rhGFR-α3 and rrGNDF from R&D Systems; rhNRTN and rhARTN from PeproTech). When referring to the use of 'GFLs', we have employed GDNF, NRTN, ARTN and their specific co-receptors in combination. LSK and HSC cells were purified by flow cytometry and stimulated overnight with GFL/GFR-α combinations to determine *Bcl2 and Bcl2l1* expression levels. For inhibition experiments cells were incubated 2 h before GFL stimulation, to test CREB phosphorylation, or during overnight stimulation with GFLs, to determine *Bcl2 and Bcl2l1* expression levels, with SB 202190 and PD98,059 from Sigma-Aldrich or Akt1/2, Akt InhibitorVIII and CBP-CREB Interaction Inhibitor from Calbiochem. To detect Annexin V, 4×10^4 E14.5 WT, *Ret*$^{-/-}$ *Ret*$^{+/BCLxL}$ or *Ret*$^{BCLxL/BCLxL}$ Lin$^-$cKit$^+$ cells per well were cultured overnight in DMEM alone or with GFL/GFR-α. Lin$^-$Sca1$^+$cKit$^+$ cells were stimulated with GFL/GFR-α for 120 h and sequentially analysed by flow cytometry.

Haematopoietic stem cell expansion and transplantation. FACS-sorted murine HSCs were cultured for 7 days in StemSpan SFEM (STEMCELL Technologies) with recombinant mSCF (PeproTech), mTPO (R&D Systems) and in the presence or absence of 500 ng ml^{-1} each of GFL and co-receptor (rrGFR-α1, rmGFR-α2, rhGFR-α3 and rrGNDF from R&D Systems; rhNRTN and rhARTN from PeproTech). Human cord blood CD34$^+$ cells were cultured similarly to murine HSCs, adding rmFLT3. Expanded cells were then transplanted in competition with CD45.1 bone marrow into lethally irradiated CD45.1 mice (murine) or into NSG mice irradiated with 250 rad (human). All human samples were obtained with informed consent

and protocols were approved by the Centro Hospitalar Lisboa Norte/Faculdade de Medicina de Lisboa Health Ethics Committee.

Real-time PCR analysis. RNA was extracted from cell suspension using RNeasy Mini Kit or RNeasy Micro Kit (Qiagen). Real-time PCR for *Ret*, *Gfra1*, *Gfra2* and *Gfra3* was done as previously described[6,34]. *Hprt1* was used as housekeeping gene. For TaqMan assays (Applied Biosystems) RNA was retro-transcribed using a High Capacity RNA-to-cDNA Kit (Applied Biosystems), followed by a pre-amplification PCR using TaqMan PreAmp Master Mix (Applied Biosystems). TaqMan Gene Expression Master Mix (Applied Biosystems) was used in real-time PCR. TaqMan Gene Expression Assays bought from Applied Biosystems were the following: Gapdh Mm99999915_g1; *Hprt1* Mm00446968_m1; *Gusb* Mm00446953_m1; *Mpl* Mm00440310_m1; *Mcl1* Mm00725832_s1; *Meis1* Mm00487664_m1; *Angpt1* Mm00456503_m1; *Eya1* Mm00438796_m1; *Eya2* Mm00802562_m1; *Egr1* Mm00656724_m1; *Tek* Mm00443243_m1; *Slamf1* Mm00443316_m1; *Lef1* Mm00550265_m1; *Thy1* Mm00493681_m1; *Mllt3* Mm00466169_m1; *Hoxa5* Mm00439362_m1; *Hoxa9* Mm00439364_m1; *Hoxc4* Mm00442838_m1; *Pbx3* Mm00479413_m1; *Ndn* Mm02524479_s1; *Evi1* Mm00514814_m1; *Mll1* Mm01179213_g1; *Hlf* Mm00723157_m1; *Cxcr4* Mm01292123_m1; *Smo* Mm01162710_m1; *Igf2r* Mm00439576_m1; *Cdkn1a* Mm00432448_m1; *Notch1* Mm00435249_m1; *Kitl* Mm00442972_m1; *Thpo* Mm00437040_m1; *Bcl2l1* Mm00437783_m1; *Bcl2* Mm00477631_m1; *Pspn* Mm00436009_g1; *Artn* Mm00507845_m1; *Nrtn* Mm03024002_m1; *Gdnf* Mm00599849_m1; *Ret* Mm00436304_m1. For HSC signature gene arrays, gene expression levels were normalized to *Gapdh*, *Hprt1* and *Gusb*. For *Bcl2*/*Bcl2l1* expression after HSC stimulation and *Ret* expression levels after *in vivo* transfer, gene expression levels were normalized to *Gapdh* and *Hprt1*. Real-time PCR for human samples used the following primers: *GAPDH* AGGTGAAGGTCGGAGTCAAC and TCTCCATGGTGGTGAAGACG; *BCL2* GCACCTGCACACCTGGAT and CCAAACTGAGCAGAGTCTTCAG; *BCL2L1* AGCCTTGGATCCAGGAGAAC and AGCGGTTGAAGCGTTCCT.

Statistics. Statistical analysis used Microsoft Excel. Variance was analysed using *F*-test. Student's *t*-test was performed on homocedastic populations, and Student's *t*-test with Welch correction was applied on samples with different variances. When comparing more than two samples, one-way ANOVA was employed. We analysed Kaplan–Meier survival curves with a log rank test. *, ** and *** represent *P* values lower than 0.05, 0.01 and 0.001, respectively.

30. Mombaerts, P. *et al.* RAG-1-deficient mice have no mature B and T lymphocytes. *Cell* **68,** 869–877 (1992).
31. Uesaka, T. & Enomoto, H. Neural precursor death is central to the pathogenesis of intestinal aganglionosis in Ret hypomorphic mice. *J. Neurosci.* **30,** 5211–5218 (2010).
32. Kunisaki, Y. *et al.* Arteriolar niches maintain haematopoietic stem cell quiescence. *Nature* **502,** 637–643 (2014).
33. van de Pavert, S. A. *et al.* Maternal retinoids control type 3 innate lymphoid cells and set the offspring immunity. *Nature* **508,** 123–127 (2014).
34. Peixoto, A. *et al.* CD8 single-cell gene coexpression reveals three different effector types present at distinct phases of the immune response. *J. Exp. Med.* **204,** 1193–1205 (2007).

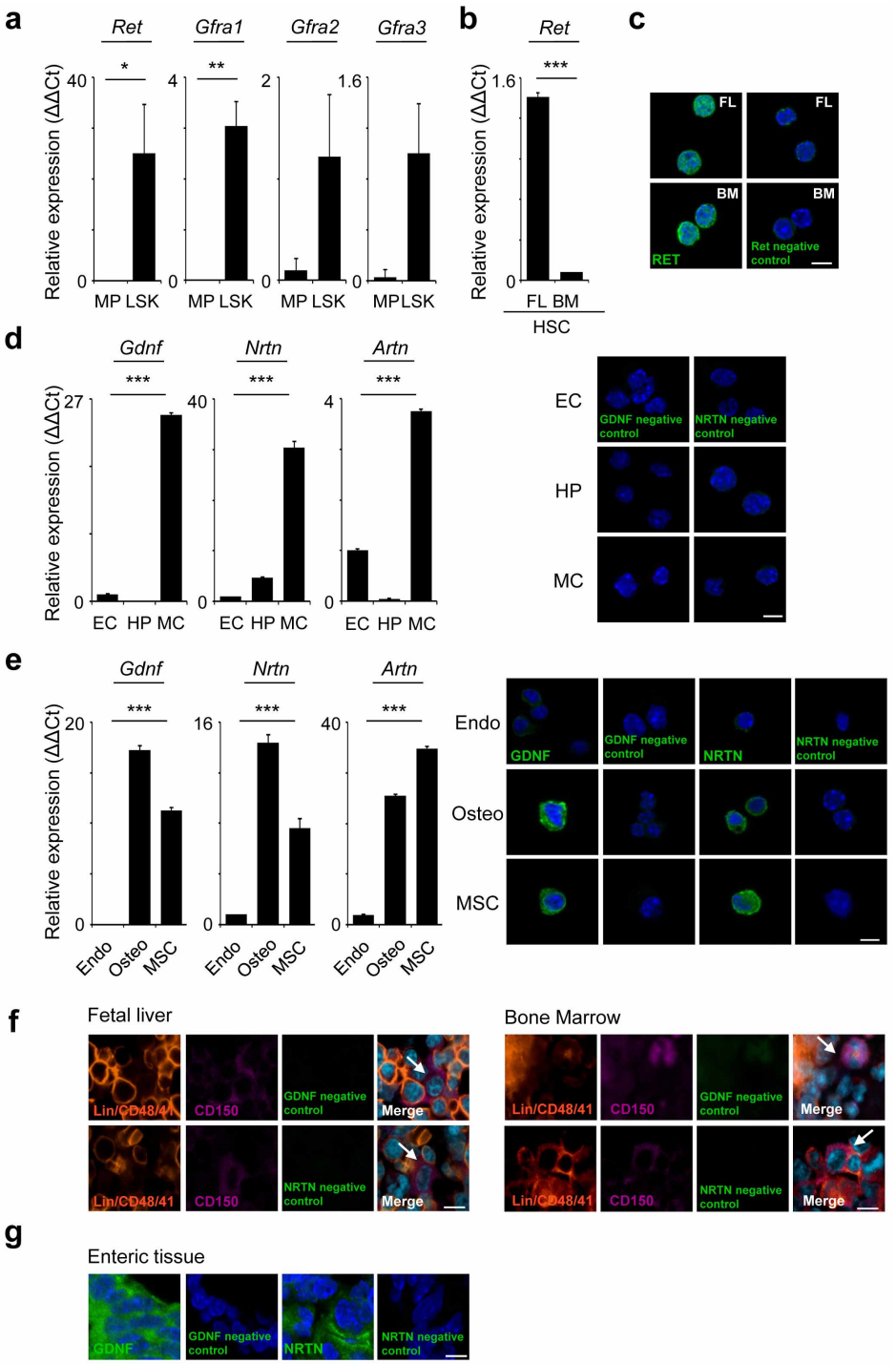

Extended Data Figure 1 | *Ret* expression in haematopoietic progenitors and *Ret* ligand expression in the fetal and adult HSC environment. **a**, FACS-sorted E14.5 fetal liver myeloid progenitors and LSK were analysed by RT–qPCR. **b**, FACS-sorted HSCs from E14.5 fetal liver and adult bone marrow were analysed by RT–qPCR. **c**, FACS-sorted E14.5 fetal liver and adult bone marrow HSCs were analysed by confocal microscopy. **d**, E14.5 fetal liver TER119$^-$CD45$^-$CD31$^+$ endothelial cells (EC), TER119$^-$CD45$^-$CD31$^-$ cKit$^+$ICAM-1$^-$ hepatocyte progenitor cells (HP) and TER119$^-$CD45$^-$CD31$^-$ cKit$^-$ICAM-1$^+$ mesenchymal cells (MC) were analysed by RT–qPCR (left); negative controls relative to Fig. 1c were analysed by confocal microscopy (right). **e**, Bone marrow TER119$^-$CD45$^-$CD31$^+$Sca1$^+$ endothelial cells (Endo), TER119$^-$CD45$^-$CD31$^-$Sca1$^-$CD51$^+$ osteoblasts (Osteo) and TER119$^-$CD45$^-$CD31$^-$Sca1$^+$CD51$^+$ mesenchymal stem cells (MSC) were analysed by RT–qPCR (left) and by confocal microscopy (right). **f**, E14.5 fetal liver and adult bone marrow were analysed by confocal microscopy. Arrows, candidate Lin$^-$CD150$^+$CD48$^-$CD41$^-$ HSCs, relative to Fig. 1d, e. Figure shows negative controls for GFL staining. **g**, E15.5 gut tissue was analysed by confocal microscopy. White bar, 5 μm. Error bars, s.e.m. Housekeeping genes: *Gapdh* and *Hprt1*. ***P value for one-way ANOVA lower than 0.001.

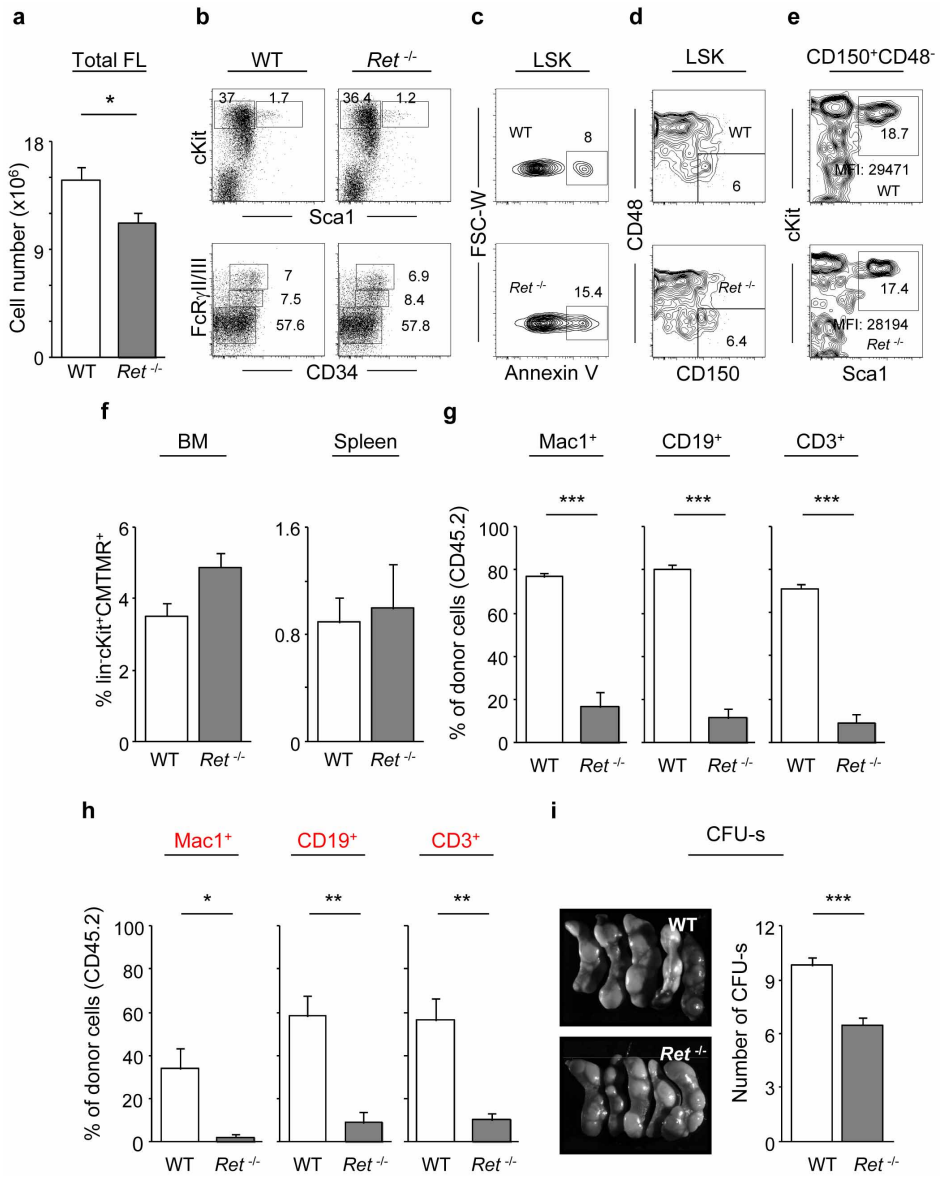

Extended Data Figure 2 | LSKs are affected by *Ret* deficiency and have reduced reconstitution capacity. **a**, E14.5 total fetal liver cells. WT $n = 20$; $Ret^{-/-}$ $n = 18$. **b**, Flow cytometry analysis of E14.5 $Ret^{-/-}$ and WT littermate control LSKs (top) and myeloid progenitors (bottom). **c**, Flow cytometry analysis of Annexin V^+ cells in cultured LSK cells. **d**, Flow cytometry analysis of E14.5 $Ret^{-/-}$ and WT littermate control HSCs. **e**, Flow cytometry analysis of E14.5 $Ret^{-/-}$ and WT $Lin^-CD150^+CD48^-$ HSC cells. Mean fluorescence intensity of cKit was analysed. No statistically significant differences were found. **f**, Lin^-cKit^+ cells were labelled with CMTMR. Percentage of $Lin^-cKit^+CMTMR^+$ cells in bone marrow and spleen 20 h after injection ($n = 3$). **g**, **h**, Percentage of donor CD45.2 cells in blood cell lineages 16 weeks after primary and secondary (red) transplantation, relative to Fig. 2b, d. **i**, Day 12 CFU-s. WT $n = 10$; $Ret^{-/-}$ $n = 10$. Error bars, s.e.m. *, ** and ***, *P* values for Student's *t*-test lower than 0.05, 0.01 and 0.001 respectively.

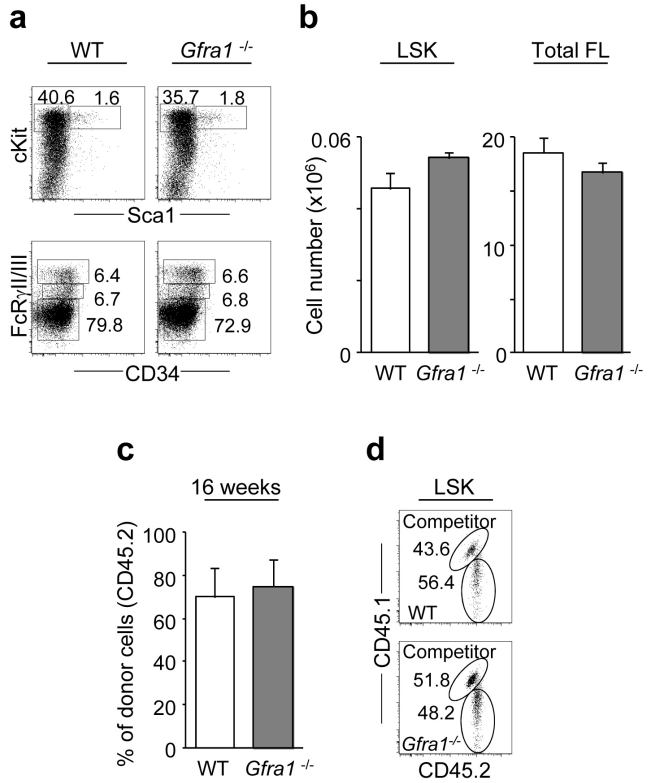

Extended Data Figure 3 | *Gfra1*-deficient embryos have normal LSK numbers and reconstitution potential. **a**, Flow cytometry analysis of E14.5 *Gfra1*$^{-/-}$ and WT littermate control LSKs (top) and myeloid progenitors (bottom). **b**, Number of LSKs and total fetal liver cells. WT $n = 9$; *Gfra1*$^{-/-}$ $n = 10$. **c**, *Gfra1*$^{-/-}$ or WT cells were injected with a third-party CD45.1/2 competitor. Percentage of donor CD45.2 cells in blood 16 weeks after transplantation. WT $n = 5$; *Gfra1*$^{-/-}$ $n = 3$. **d**, Flow cytometry analysis of bone marrow LSK cells 16 weeks after transplantation. Error bars, s.e.m.

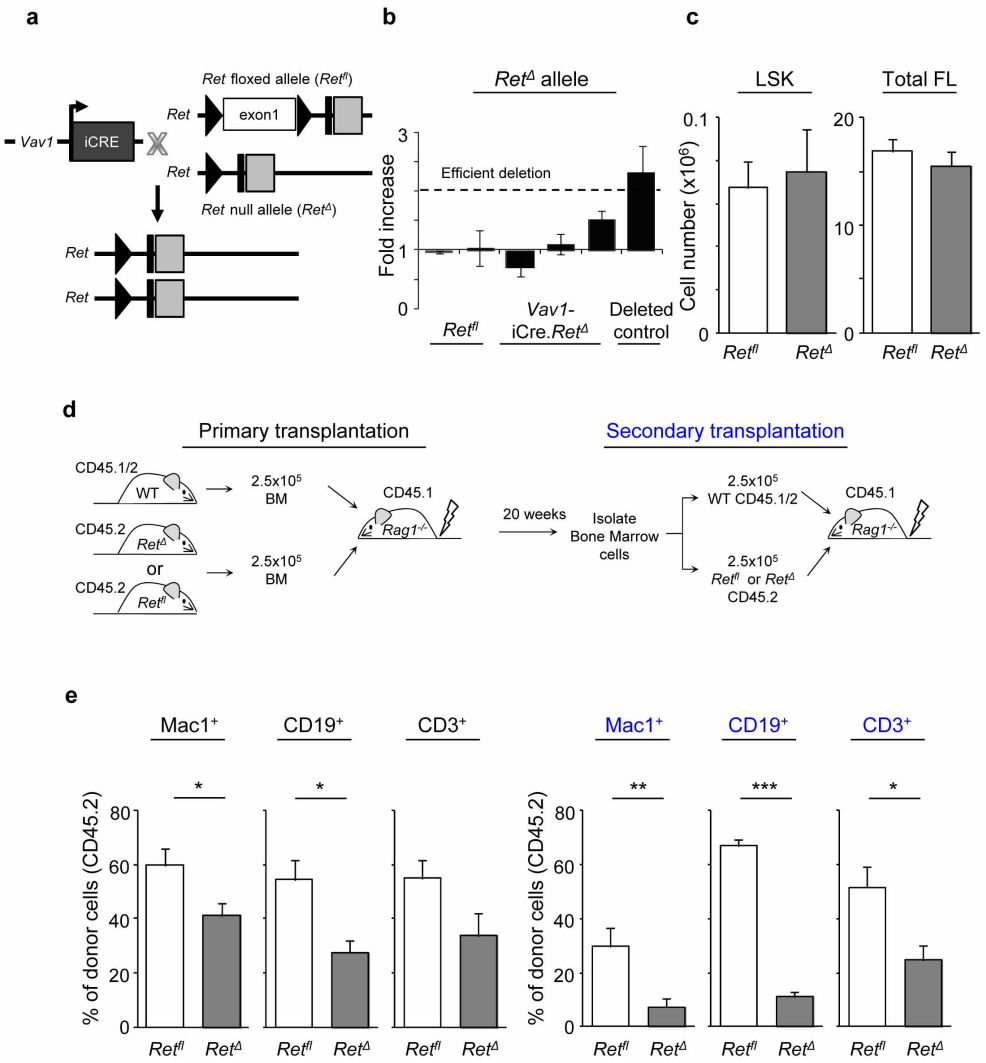

Extended Data Figure 4 | *Ret* conditional knockout mice and analysis of haematopoietic stem cells. **a**, *Ret* conditional knockout. Scheme of the targeted *Ret* allele. **b**, E14.5 fetal liver HSCs from Ret^{fl} littermate controls (two animals) and Ret conditional knockout *Vav1*-iCre.Ret^{Δ} (three animals) and deleted bone marrow control (last column) were purified by flow cytometry. Efficient deletion of *Ret* in *Vav1*-iCre.Ret^{Δ} cells was determined by qPCR as fold increase relative to littermate control cells. **c**, Number of E14.5 LSKs and total fetal liver cells. Ret^{fl} $n = 8$; Ret^{Δ} $n = 8$. **d**, Scheme of competitive transplantation with Ret^{Δ} animals and littermate controls, relative to Fig. 2h. **e**, Percentage of donor CD45.2 cells in blood cell lineages 16 weeks after primary and secondary transplantation. Error bars, s.e.m. *, ** and ***, *P* values for Student's *t*-test lower than 0.05, 0.01 and 0.001 respectively.

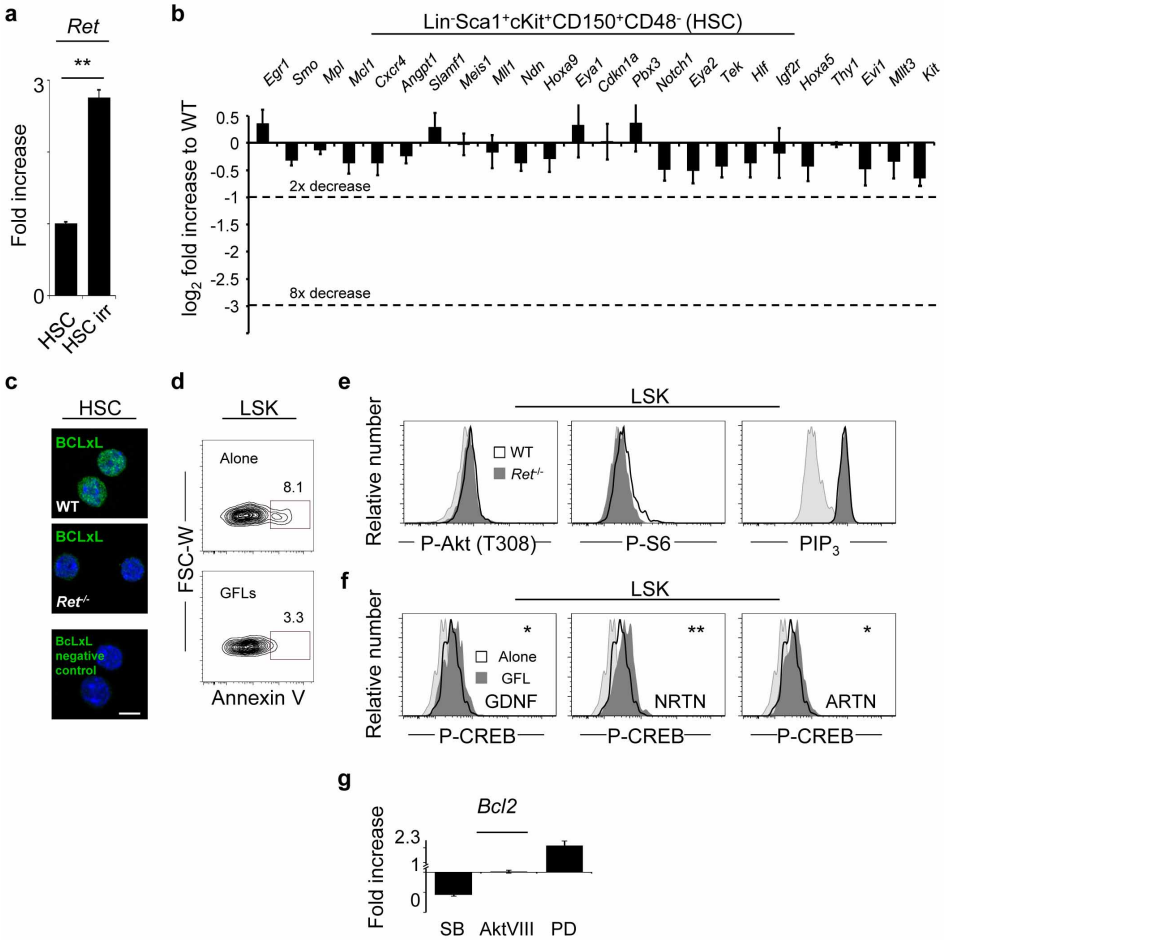

Extended Data Figure 5 | *Ret* expression increases after haematopoietic stress, and RET signalling increases CREB phosphorylation and cell survival. **a**, Mice were sublethally irradiated. Irradiation-induced stressed HSCs were purified by flow cytometry at 72 h and analysed by RT–qPCR. **b**, RT–qPCR for fetal liver E14.5 $Ret^{-/-}$ and WT HSCs ($n = 3$). **c**, Confocal analysis of BCLxL expression in WT and $Ret^{-/-}$ HSCs. **d**, Flow cytometry analysis of Annexin V^+ cells in cultured LSK cells. **e**, Flow cytometry of E14.5 $Ret^{-/-}$ and WT littermate controls. P-Akt (T308), P-S6 and PIP_3: WT $n = 6$, $Ret^{-/-}$ $n = 6$. **f**, Flow cytometry analysis of LSK cells in the absence or presence of GDNF, NRTN or ARTN for 1 h ($n = 6$). **g**, *Bcl2* expression in LSK cells upon GFL treatment and with different inhibitors, relative to LSKs treated with GFLs only. Light grey, isotype control. White bar, 5 µm. Error bars, s.e.m. * and **, *P* values for Student's *t*-test lower than 0.05 and 0.01 respectively.

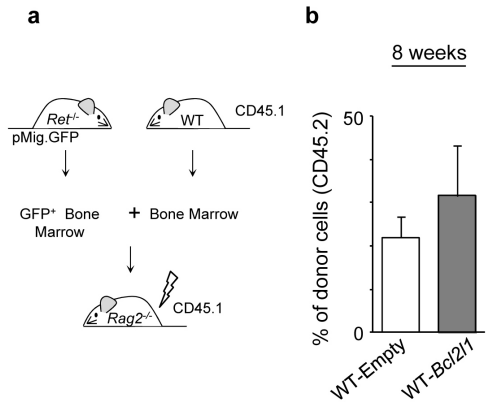

Extended Data Figure 6 | Rescue of haematopoietic progenitors with *Ret* and its downstream targets. **a**, Scheme of competitive transplantation, relative to Fig. 4b, c. **b**, Flow cytometry analysis of donor CD45.2 blood cells at 8 weeks upon transplantation of *Bcl2l1*-transduced WT haematopoietic progenitor cells. Error bars, s.e.m.

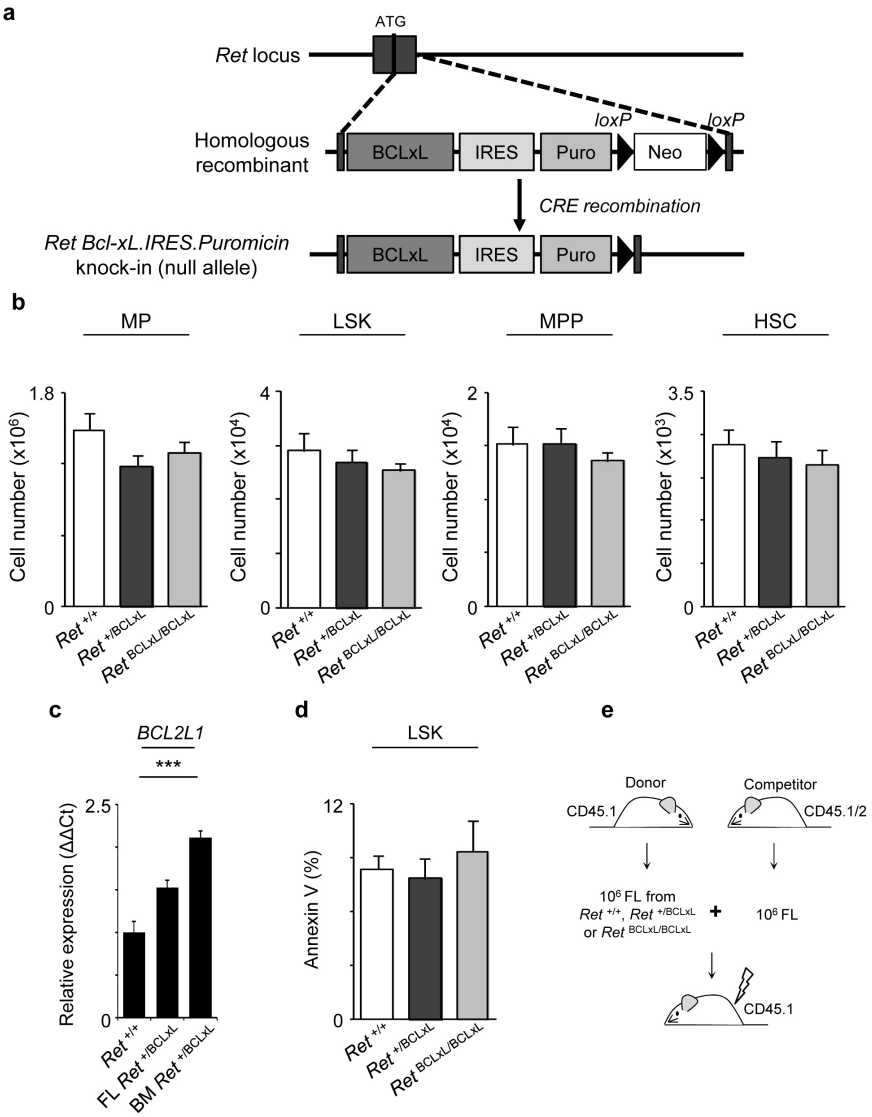

Extended Data Figure 7 | Generation and analysis of *Ret*^{BCLxL} mice. **a**, *Ret* locus was targeted by a construct containing the BCLxL coding sequence, an internal ribosomal entry site (IRES) and a puromycin resistance cassette, followed by a floxed neomycin resistance cassette to aid negative selection. *Ret* Bcl-xL.IRES.Puromicin knock-in mice were obtained by excising of the neomycin cassette. **b**, Number of myeloid progenitors, LSK cells, multipotent progenitor cells and HSCs in E14.5 fetal liver. WT $n = 7$; $Ret^{+/BCLxL}$ $n = 9$; $Ret^{BCLxL/BCLxL}$ $n = 8$. **c**, FACS-sorted HSCs from $Ret^{+/+}$, E14.5 fetal liver $Ret^{+/BCLxL}$ and adult bone marrow $Ret^{+/BCLxL}$ were analysed by RT–qPCR for human *BCL2L1* expression. Housekeeping genes: *Gapdh* and *Hprt1*. **d**, Annexin V^{+} cells in cultured E14.5 LSK cells. WT $n = 6$; $Ret^{+/BCLxL}$ $n = 4$; $Ret^{BCLxL/BCLxL}$ $n = 6$. **e**, Scheme of competitive transplantation. $Ret^{BCLxL/BCLxL}$ animals and littermate controls were injected in competition with CD45.1/CD45.2 cells, relative to Fig. 4d, e. Error bars, s.e.m. ***P value for one-way ANOVA lower than 0.001.

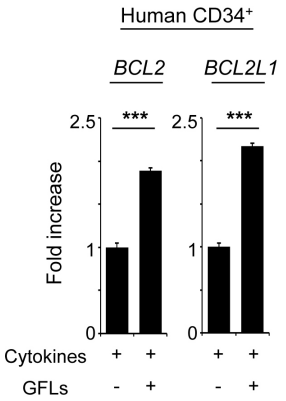

Extended Data Figure 8 | GFLs increase anti-apoptotic gene expression in human haematopoietic progenitors. Human cord blood $CD34^+$ cells were cultured in the presence or absence of GFLs for 4 days and analysed by RT–qPCR. Gene expression relative to cells cultured without GFLs. Error bars, s.e.m. ***P values for Student's t-test lower than 0.001.

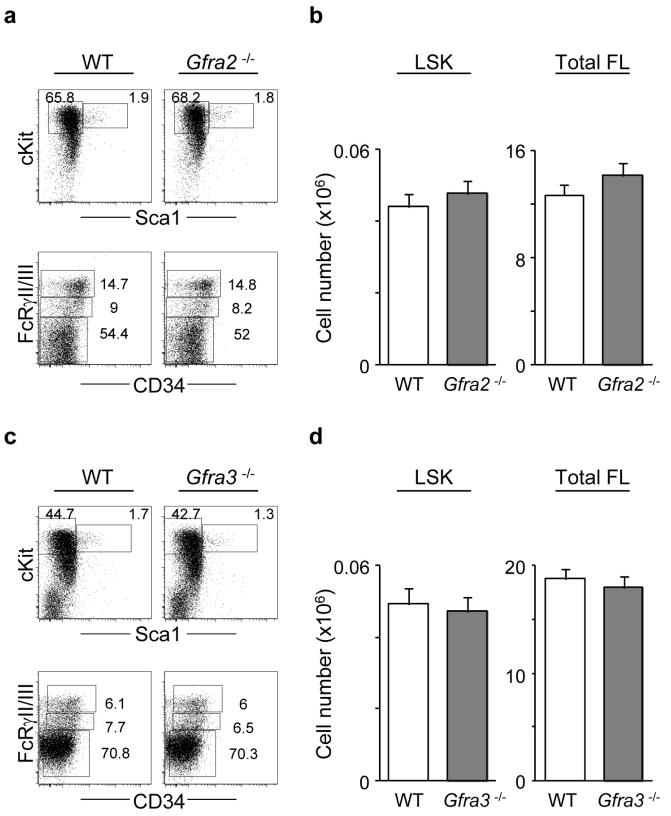

Extended Data Figure 9 | *Gfra2*- and *Gfra3*-deficient embryos have normal haematopoietic progenitors. **a**, Flow cytometry analysis of E14.5 *Gfra2*$^{-/-}$ and WT littermate control LSKs (top) and myeloid progenitors (bottom). **b**, Number of LSKs and total fetal liver cells. WT $n = 12$; *Gfra2*$^{-/-}$ $n = 11$. **c**, Flow cytometry analysis of E14.5 *Gfra3*$^{-/-}$ and WT littermate control LSKs (top) and myeloid progenitors (bottom). **d**, Number of LSKs and total fetal liver cells. WT $n = 11$; *Gfra3*$^{-/-}$ $n = 20$. Error bars, s.e.m.

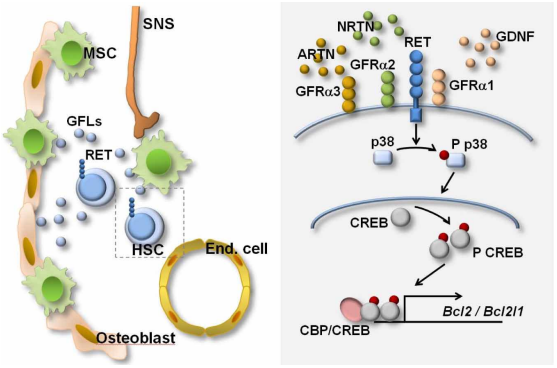

Extended Data Figure 10 | Neuronal growth factors regulate HSC response to physiological demand. The neurotrophic factors GDNF, NRTN and ARTN are produced by cells in the HSC microenvironment and act directly on HSCs by activation of RET. Highlighted area: RET stimulation results in p38/MAP kinase and CREB activation leading to *Bcl2* and *Bcl2l1* expression. RET signals provide HSCs with survival signals that preserve HSC stemness.